Int. J. Radiation Oncology Biol. Phys., Vol. 61, No. 5, pp. 1535–1550, 2005

0360-3016/05/$–see front matter

ELSEVIER

doi:10.1016/j.ijrobp.2004.11.037

PHYSICS CONTRIBUTION

FOUR-DIMENSIONAL IMAGE-BASED TREATMENT PLANNING: TARGET VOLUME SEGMENTATION AND DOSE CALCULATION IN THE PRESENCE OF RESPIRATORY MOTION

EIKE RIETZEL, PH.D.,*† GEORGE T. Y. CHEN, PH.D.,* NOAH C. CHOI, M.D.,* AND CHRISTOPHER G. WILLET, M.D.*

*Department of Radiation Oncology, Massachusetts General Hospital, Harvard Medical School, Boston, MA;
†Abteilung Biophysik, Gesellschaft für Schwerionenforschung, Darmstadt, Germany

Purpose: To describe approaches to four-dimensional (4D) treatment planning, including acquisition of 4D-CT scans, target delineation of spatio-temporal image data sets, 4D dose calculations, and their analysis.
Methods and Materials: The study included patients with thoracic and hepatocellular tumors. Specialized tools were developed to facilitate visualization, segmentation, and analysis of 4D-CT data: maximum intensity volume to define the extent of lung tumor motion, a 4D browser to examine and dynamically assess the 4D data sets, dose calculations, including respiratory motion, and deformable registration to combine the dose distributions at different points.
Results: Four-dimensional CT was used to visualize and quantitatively assess respiratory target motion. The gross target volume contours derived from light breathing scans showed significant differences compared with those extracted from 4D-CT. Evaluation of deformable registration using difference images of original and deformed anatomic maps suggested the algorithm is functionally useful. Thus, calculation of effective dose distributions, including respiratory motion, was implemented.
Conclusion: Tools and methods to use 4D-CT data for treatment planning in the presence of respiratory motion have been developed and applied to several case studies. The process of 4D-CT–based treatment planning has been implemented, and technical barriers for its routine use have been identified. © 2005 Elsevier Inc.

Four-dimensional (4D) computed tomography, 4D treatment planning, treatment planning, target volumes, organ motion.

INTRODUCTION

Variations in organ shape and position can occur on both an interfractional and an intrafractional time scale. Sources of interfractional change include tumor shrinkage or growth, weight changes, and variations in organ filling (e.g., bowel/bladder variations). Sources of intrafractional motion include peristalsis, cardiac motion, and respiration.

These temporal anatomic changes can introduce significant errors in imaging, treatment planning, and treatment delivery. Imprecise knowledge of the target shape and trajectory imposes a strategy of larger field margins, resulting in suboptimal dose conformation. Ideally, accurate organ motion would be included explicitly in treatment planning, on a patient-specific basis to determine its effect on the delivered dose. The focus of this article was to frame the important elements of treatment planning in the presence of respiration-induced organ motion. We analyzed and report our experience concerning the effects of respiratory motion on target delineation, dose calculation, and dose–volume histogram (DVH) analysis using newly available volumetric temporal imaging. The anatomic sites included tumors in the thorax and abdomen.

Treatment planning is frequently based on a single computed tomography (CT) scan, taken during light breathing. Respiratory motion during CT data acquisition can induce severe motion artifacts, resulting in inaccurate assessment of organ shape and location (1–4). To reduce such artifacts, CT data may be acquired during breath holds (5) or by

Reprint requests to: Eike Rietzel, Ph.D., Department of Radiation Oncology, Northeast Proton Therapy Center, Massachusetts General Hospital, 30 Fruit St., Boston, MA 02114. Tel: (617) 726-8153; Fax: (617) 726-3603; E-mail: eike@rietzel.net

Presented in part at ASTRO 2003, Salt Lake City, UT.

Supported by NCI-PO1 Grant 21239 and in part by Deutsche Forschungsgemeinschaft in cooperation with Gesellschaft für Schwerionenforschung (stipend to E.R.).

Acknowledgments—The authors acknowledge the technical support of General Electric Medical Systems and Varian Medical Systems in the acquisition of four-dimensional CT data; give special thanks to the members of the Department of Radiation Oncology who provided treatment planning and contouring expertise, including Thomas Harris, Judith Adams, and Jonathan Jackson; and acknowledge Andrzej Niemierko for the calculation of EUDs.

Received Mar 22, 2004, and in revised form Nov 15, 2004. Accepted for publication Nov 18, 2004.

gating at a specific respiratory phase during imaging (6). Additional data on patient-specific respiratory motion can be obtained by fluoroscopy (7). However, fluoroscopy is limited to planar projections of anatomy. To obtain volumetric three-dimensional (3D) anatomic data during respiration, a time-resolved CT data acquisition protocol is needed.

Once volumetric anatomic maps are acquired, the process of target and normal organ segmentation can begin. Typically, the gross target volume (GTV) is outlined on the treatment-planning scan. This volume is then expanded to a clinical target volume (CTV) to include suspected microscopic spread (8). To ensure sufficient dose coverage of the CTV throughout the treatment course, margins are added to include the geometric uncertainties. Using the new nomenclature of International Commission on Radiation Units and Measurements (ICRU) Report 62 (9), the CTV is expanded to an internal target volume to account for internal target motion; the internal target volume is subsequently expanded to a planning target volume (PTV) to incorporate the daily setup uncertainties.

Geometric margins to account for respiratory motion are usually derived from a combination of experience, direct observation at simulation (e.g., via fluoroscopy), or using values reported in the literature (10). Such margins are tumor site specific, but generally not patient specific. Stevens *et al.* (11) and van Sörnsen *et al.* (12) have reported that the tumor location cannot reliably predict the mobility of lung tumors. Although patient-specific target motion can be assessed through two-dimensional projections by fluoroscopy (7), it has its limitations. Studies of patients with abdominal tumors clipped with radiopaque markers have provided data on clip motion only, not explicitly on the regions of the target (or unclipped normal organs). In a retrospective study of treatments of hepatocellular tumors, Rosu *et al.* (13) reported significant changes in the liver dose if organ motion were included in the dose calculations. Their dose calculations were based on a single breath-hold CT scan and a dose convolution method in which patient-specific motion was obtained by fluoroscopy. To calculate the dose distributions, including temporal anatomic changes in three dimensions, time-resolved CT is needed.

Four-dimensional (4D)-CT data provide the primary image data needed to include explicitly patient-specific respiratory motion into treatment planning to ensure dose coverage of the target throughout the breathing cycle and to calculate the dose distributions for the targets and organs at risk when respiratory motion is present during beam delivery. The accuracy of the 4D-CT scan protocol has been validated through phantom studies and has been reported in detail elsewhere (14). Our initial patient imaging study involved 4D-CT scans of 20 patients, 10 with abdominal tumors and 10 with thoracic tumors. Given these data, issues of data acquisition, assessment of organ motion, dose calculation, and analysis were studied. The explicit inclusion of time-resolved patient data altered the standard workflow of radiotherapy (RT) planning. We report on 4D-CT scanning at Massachusetts General Hospital (MGH) and discuss how the conventional workflow for treatment planning was altered to use 4D-CT.

METHODS AND MATERIALS

4D CT scanning

The initial work on 4D-CT has been previously reported (15–17). The common underlying principle in these approaches has been to acquire axial/helical tomographic images while simultaneously recording the respiratory breathing pattern. These data are then reorganized (resorted) to generate multiple spatiotemporally coherent anatomic data sets.

The 4D-CT scan process used in this study was developed by General Electric Medical Systems (18). CT data were acquired on a General Electric Lightspeed Qx/i 4-slice scanner in axial cine mode. The scanner continuously acquires projection data at each couch position for an interval equal to the patient's respiratory period plus the interval needed for one CT tube rotation (0.8 s for our CT scanner). The beam is then turned off, and the table is advanced to the next scan position. This is repeated until full longitudinal coverage of the region of interest has been obtained. In the reconstruction process, approximately 20–25 images are reconstructed per slice, evenly distributed throughout the respiratory period. Each reconstructed axial image represents the anatomy at a different instant during the patient's respiratory cycle. Typically, a total of 1000–1500 images are acquired during a 4D-CT study. Once the scan setup parameters have been determined, the 4D data acquisition and image reconstruction process is fully automated. The elapsed time required to cover 25 cm longitudinally with a breathing period of 5 s is about 2.5 min on a four-slice CT scanner.

Patient respiratory cycle data are needed to generate spatiotemporally consistent image data. During CT scanning, the patient's abdominal surface motion is recorded with the Varian RPM system (19–21). In brief, the RPM system illuminates infrared reflecting dots on a plastic marker block placed on the patient's abdomen. A CCD camera with an infrared filter records the abdominal surface motion (~30 Hz). RPM software tracks the marker trajectory in real time and calculates the respiratory phase on the basis of signal processing of the observed amplitude. The CT scanner and RPM system communicate during data acquisition via a transistor-transistor logic (TTL) signal to indicate when the CT X-ray beam is turned on or off.

The reconstructed axial images and RPM respiratory data are transferred to an Advantage Windows workstation at which Advantage4D Software (General Electric, Milwaukee, WI) is used to sort images retrospectively into the desired respiratory phases. On the basis of the temporal correlation between the surface motion and image data acquisition, a specific respiratory phase is assigned to each image. The user chooses a desired respiratory phase. An axial image at a given couch position is binned on the basis of its respiratory phase. Ideally, a complete volumetric image data set at a given respiratory phase interval is generated through this process. This step is repeated for different respiratory phases to generate multiple (~10–20) volumetric, spatio-temporally consistent CT volumes. Data sets are labeled by the percentage of the respiratory cycle, with 0% corresponding to inhalation and 50% to exhalation. Relative respiratory phases are uniformly spaced in time within a respiratory cycle.

The accuracy of 4D-CT imaging, its ability to reduce imaging

artifacts in organ shape, and its ability to track the centroid of moving objects has been established and reported in detail elsewhere (14). On the basis of these studies, the initial data acquisition protocol was modified. Improved 4D-CT data sets can be obtained if as many images as possible are reconstructed at each couch position. The recommended number of images at a couch position is >20. As a result, more temporally consistent binning of images at a given respiratory phase can be achieved. The geometric imaging accuracy is then about one slice thickness (2.5 mm) for periodic motion. Residual volumetric differences between spherical objects (radius ~2 cm) scanned helically and static or with 4D-CT while moving are within ~5%. The total number of images that can be reconstructed with our scanner is currently limited to 1500 per study. Therefore, it is necessary to balance the region longitudinally scanned with the number of images reconstructed per couch position. In principle, the scan length is not limited, but it determines the maximal number of reconstructed images per couch position and, therefore, the temporal resolution.

The patient dose during 4D-CT scanning is greater than during standard scanning. For a given peak-kilo-voltage (kVp) and milli-Ampere setting, the increase in dose relative to standard axial CT scans is a function of the cine duration determined by the patient's respiratory period and the tube rotation time. For example, for a patient with a respiratory period of 4.2 s, the cine duration would be set to 5 s. With a tube rotation time of 0.8 s, this leads to a relative dose increase by a factor of 6.25. From our practical experience, this factor can be reduced for most patients without significant image degradation if the milli-Ampere is reduced.

Motion analysis tools

Four dimensional-CT generates ~20 times more image data than a standard planning scan. Clearly, this provides challenges in image processing and treatment planning. New tools are needed to view tumor and normal organ motion effectively to deal with issues of deformable registration, dose calculation, and DVH analysis. Key methods are described in this section.

Visualization of 4D data

An initial assessment of organ motion was made by generating animations that display anatomy at different respiratory phases in selected axial, sagittal, and coronal planes. Because animation software was not available in the treatment planning software, we used screen captures of a selected imaging plane at multiple points in the respiratory cycle. These images were then concatenated to form animations. Although such movies provided a dynamic display of the anatomy during respiration, the process was tedious and time consuming. Therefore, a more efficient method of assessing and studying the motion of the tumor and normal organs was designed. A 4D browser program was written by one of us (E.R.) to facilitate fast visualization. The personal computer-based browser loads the entire set of 4D-CT volumes (~500 MB of data) and interactively displays the selected axial, sagittal, or coronal planes, cycling through the respiratory phase. This allows for visualization of a manual selection of a specific respiratory phase or a movie loop of the entire data set.

Quantitative analysis

To facilitate quantitative motion analysis, the volumes of interest were manually contoured at each respiratory phase of a 4D-CT study. One of the limiting factors in 4D analysis is the substantial increase in workload, given that the number of CT images requiring processing is increased by a factor of ≥10. Segmentation for the initial cohort of patients was performed manually by MGH staff. From these manually contoured organs and tumor volumes, the maximal excursions of motion and centroid trajectory were determined.

A composite target volume is the union of individual target volumes at different instants in time, and it is useful when treatment is to be delivered during a portion of, or the entire, respiratory cycle. Generation of composite target volumes on the basis of the inhale and exhale breath hold CT scans has recently been reported by Allen *et al.* (22). To define explicitly a composite target volume from 4D-CT data, the standard approach would include contouring GTVs on all 10 data sets. At a minimum, an estimate of the composite GTV may be derived from contouring the GTV on the volumes nearest inhale and exhale and fusing them. If the GTVs are contoured on these extrema data sets, overlaying the composite contours onto each breathing phase and visually verifying adequate coverage could establish verification that the composite volume includes all instances of GTVs at other respiratory phases. Given a possible phase shift between internal organ motion and external abdominal surface motion, the extrema of tumor positions must be selected by visual inspection.

Organ motion can also be quantified in 4D-CT when radiopaque markers are placed in the volume of interest. Most of the liver cancer patients in this study also had multiple radiopaque markers implanted around the tumor periphery. Digitization of these markers in the scan data at varying phases of respiration provided data on clip trajectory during respiration.

Rapid segmentation of lung tumors: maximum intensity volume

Manual image segmentation/contouring of a volume of interest in multiple respiratory phases of 4D-CT image data is tolerable for research and development, but in routine clinical use, automated methods are needed to deal with the increase in image data set size.

An alternative to drawing multiple contours manually at different respiratory phases has been devised to extract the composite tumor volume efficiently from 4D-CT. When a significant density difference exists between the tumor and surrounding tissue, this difference may be exploited to decrease the contouring workload. By calculating a maximum intensity volume (MIV), the composite target volume can be outlined on a single volumetric data set. The MIV can be automatically generated from the entire 4D-CT data. This is done by assigning each voxel the greatest Hounsfield unit value from all corresponding voxels over the multiple respiratory phase image data. For a lung tumor, this results in identification and localization of high-density tumor voxels compared with lower density lung tissue voxels during the interval of breathing.

Deformable image registration

Respiration induces both rigid body translation/rotation and organ deformation. During this deformation, voxels may migrate and distort, making an assessment of the dose on a voxel-by-voxel basis problematic. Deformable image registration is a tool that can relate 4D-CT volumes at different respiratory phases to each other on a voxel-by-voxel basis. We chose to use an open source software package, VTK CISG (developed by the Computational Imaging Science Group, King's College London [23]) to provide deformable image registration.

VTK CISG provides voxel-based affine and nonrigid image registration algorithms. Affine registration involves optimizing 12

degrees of freedom, including translation, rotation, scaling, and shearing. Nonrigid image registration models local deformation using a free-form deformation model based on B-splines. The algorithm defines a regular grid of control points and deforms the underlying image by moving these control points (24) guided by the selected measure of similarity. In the case studies presented here, we chose to use the sum of squared differences as the similarity measure. The similarity between two volumes was compared by calculating the intensity differences between all corresponding voxel pairs. The sum over the squared differences was then used to measure global similarity. With a decreasing sum of squared differences, the overall similarity increases. The sum of squared differences is an appropriate similarity measure to register 4D-CT volumes. For each tissue, reconstructed densities vary only slightly owing to small volumetric deformations while mass is conserved. Compared with positional density changes resulting from tissue/organ motion between 4D-CT volumes, such variations are small. A full affine registration is performed as an initial step to assess global motion between different respiratory phases. For the following nonrigid registration, different spacings of the B-spline control grid were evaluated.

To evaluate deformable registration performance, we inspected the data after registration visually, slice by slice, either by color overlay display or by difference images. Registration was considered reasonable if the lung/chest wall boundaries, gross tumor volume, and other structures in the lung parenchyma at different respiratory phases were brought into congruence. For the case presented, we achieved good registration results by applying a series of nonrigid registrations with decreasing control grid spacing (from 20 mm to 15 mm to 10 mm). In general, a series of registrations with decreasing control grid spacings from coarse to fine can improve the registration results. Finer grid sizes offer a greater number of degrees of freedom for nonrigid warping. The lung, including the tumor, needed to be segmented and dealt with as an entity separate from chest wall and ribcage because moving and stationary regions of the body compete during the registration process (owing to the intrinsic smoothness constraints of the registration algorithm).

Dose calculations

The impact of respiratory motion on conventionally generated dose distributions has been studied for selected cases. The dose calculations were performed using the FOCUS (CMS, St. Louis, MO) treatment planning system. Treatment plan parameters were optimized to irradiate the tumor and avoid normal structures, on the basis of the volumetric anatomic description from a standard helical CT scan acquired under light breathing.

The treatment plan parameters from this conventional plan (e.g., beam angle, weight, fluence pattern for intensity-modulated RT [IMRT]) were then applied to the 4D-CT data sets. These parameters were subsequently used to recalculate the dose at different breathing phases using the corresponding 4D-CT volumes to assess the impact of respiratory motion on dose distributions.

Applying a conventional treatment plan (intended for a single CT study) to multiple patient image study sets is not supported in standard treatment planning systems. Modifications to files at the underlying Unix file system level were necessary to coax the planning system to use the time-resolved image data. Scans in our initial 4D-CT studies were limited to a longitudinal length sufficient to image the tumor motion in a craniocaudal direction. To facilitate simple copying of the treatment plans, while changing the CT data they related to only, 4D-CT volumes were padded with slices from a standard helical CT scan. For 4D treatment planning, full-length 4D-CT scans will be acquired.

In our implementation, 4D dose distributions could be calculated for all modalities available on the MGH FOCUS treatment planning system; these included 3D-conformal RT, IMRT, and proton beam therapy. The dose calculations used involved a convolution algorithm, and heterogeneity corrections were turned on. DVHs were computed for each breathing phase. These individual DVHs were used to analyze the dose coverage of the target throughout the respiratory cycle. Using deformable image registration, an effective dose distribution, taking into account voxel motion during respiration, has also been calculated. Dose distributions at different respiratory phases were added with equal weighting, because the time-varying CT data were uniformly distributed throughout a respiratory cycle.

RESULTS

Motion analysis

Figure 1 shows a coronal slice through the center of the liver for four different CT data sets, including the standard helical data acquisition during light breathing and three 4D-CT data sets at specific respiratory phases of 0%, 20%, and 40%, corresponding to inhale, mid-exhale, and end-exhale. Typical breathing artifacts were present in the standard helical scan. Specifically, the liver edges were jagged or blurred owing to organ motion during data acquisition; consecutive slices under light breathing were acquired at different phases of the patient's breathing cycle, resulting in these irregularities. The 4D-CT images of the liver were significantly smoother and more realistic. In addition, the different phases of the 4D-CT data documented the craniocaudal motion of the liver during breathing. 4D-CT images in Fig. 1 showed minimal residual motion artifacts for the displayed respiratory phases. In general, residual motion artifacts are expected to be smallest near end-exhalation and end-inhalation because of the decreased velocity.

Quantitative analysis

Respiratory motion from 4D-CT can be quantified by two approaches. In the example in Fig. 1, digitization of the coordinates of the four radiopaque gold markers implanted near the tumor provided direct trajectory values for clip motion. Alternatively, the GTV can be outlined in all 4D-CT data sets, and the GTV centroid trajectory can be determined. Superoinferior clip trajectories relative to the 4D-CT mean position, as well as the GTV centroid, were plotted in Fig. 2. The dashed lines indicate the relative GTV centroid position for the helical CT scan acquired under light breathing. This illustrates that standard helical CT scanning did not record the average target position. Motion artifacts depend on the interplay between the advancing scan plane and respiratory motion. Clip and GTV motion were in good agreement, because both plots showed superoinferior liver motion of 7.5 mm. Different amplitudes between markers suggested liver deformation during respiration. However, these differences were within one slice thickness, the resolution limit of CT data acquisition. These

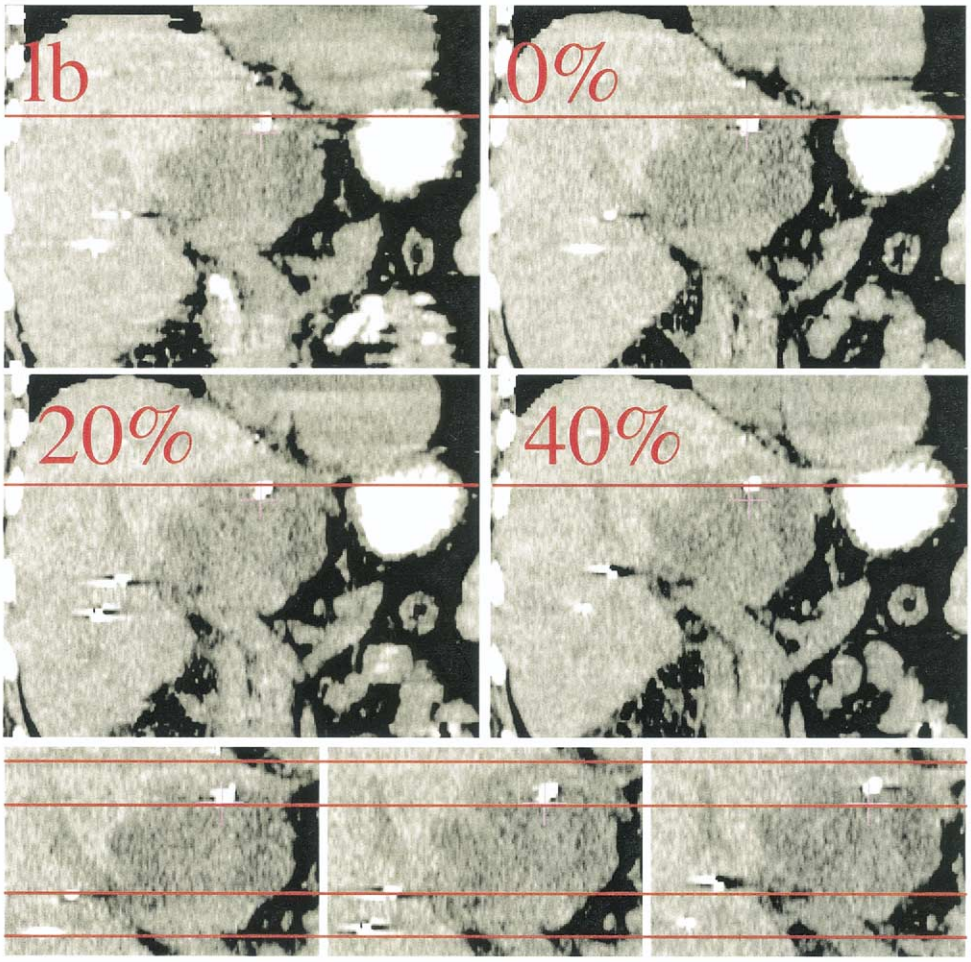

Fig. 1. Liver and hepatocellular tumor motion, same coronal slice, different data sets. Standard helical computed tomography (CT) scan acquired under light breathing (lb); 0–40%: phases of four-dimensional (4D)-CT data showing significant reduction in breathing artifacts, as well as tumor and radiopaque marker motion. (Bottom row) Zoomed target area, left to right: 0%, 20%, and 40% breathing phase. Red lines plotted to denote target motion. (4D-CT: 140 peak-kilo-voltage, 160 milli-Ampere, 15 images/slice, 0.977 × 0.977 × 2.5 mm^3).

small positional variations are well within manual contouring variations and do not necessarily represent actual target motion. Left–right and AP clip and GTV centroid motions agreed within 1–2 mm (data not shown). To date, this analysis has been performed for 3 patients. Good agreement between clip and target motion was observed in all 3 cases. Therefore, clip motion analysis seems appropriate for rapid assessment of patient-specific target motion. However, at this point, it is difficult to draw general conclusions, because the correspondence between the clip and target trajectories could depend on their relative positions.

The spatial resolution along the superoinferior axis was limited by the 2.5-mm slice thickness. On the basis of the analysis described, target volumes, including respiratory motion, can be designed with asymmetric volume expansion. However, for validation and, particularly, for dose calculations, complete 4D volumetric data at different respiratory phases is needed.

Table 1 summarizes the observed volumetric variations of the manually contoured GTV for the liver tumor at different breathing phases. The average volume of the GTV as contoured in the 4D-CT data was 256.3 cm^3 (standard deviation 11.5; 4.5%). The 296.7 cm^3 GTV on the helical CT scan was subject to significant motion artifacts. Using such an increased GTV (~16%) for treatment planning would lead to a larger treated volume. Usually, organ motion is incorporated by additional margins on the basis of experience or derived from fluoroscopy. Such margins applied to an already enlarged GTV would further increase the volume of unnecessarily treated healthy tissue.

Lung tumor motion in an example case is shown in Fig. 3. Breathing motion artifacts that distort the shape of the tumor are visible in the coronal and sagittal slices. The light breathing axial slice was most similar to the 40% phase of the 4D-CT data. Despite the continuous helical data acquisition, axial slices are in principle imaged serially. Therefore, each axial slice corresponded to one specific breathing phase. No significant distortions were found of the GTV on axial slices because of the short interval for data acquisition in the axial plane (0.8 s). However, data acquisition during breathing shuffles the order of

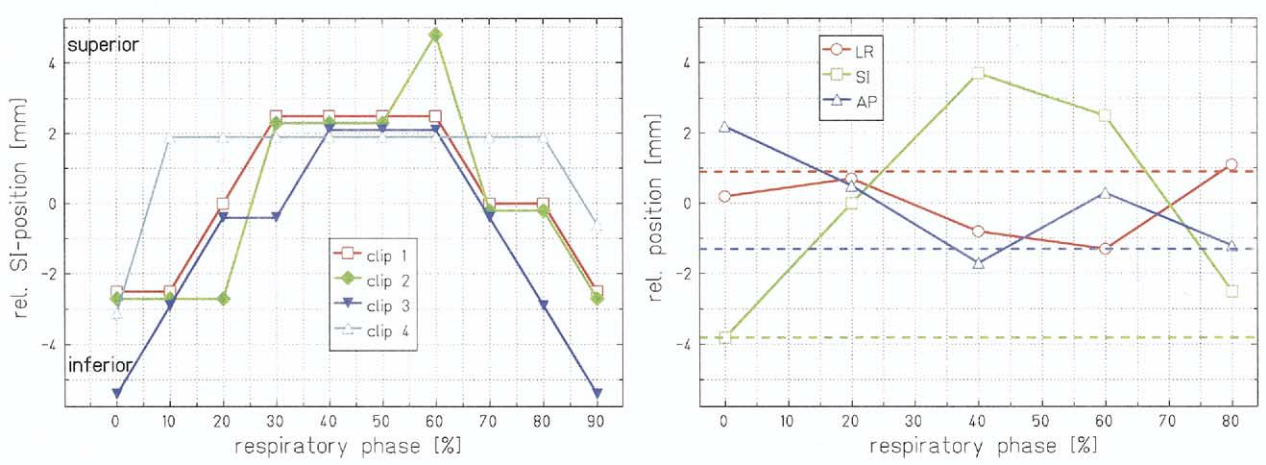

Fig. 2. Hepatocellular tumor: superoinferior marker trajectories obtained by four-dimensional computed tomography (4D-CT) analysis (left, lines slightly shifted to improve visibility) and center of gross target volume (GTV) motion (right), delineation on five breathing phases, directions of motion: right positive, superior positive, anterior positive. GTV centroid position from standard helical CT scan acquired under light breathing indicated by dashed lines. Positions plotted relative to mean position from 4D-CT.

anatomic slices in the image data, causing artifacts that are best visualized in the sagittal and coronal planes.

Gross target volume contours defined on each axial slice of the light breathing scan were overlaid on the multiplanar reconstructed sagittal and coronal sections of Fig. 3 (first column images). A composite contour derived from the union of all GTV contours from each of the 10 phases of 4D-CT data were overlaid on the 0%, 20%, and 40% data sets. On the basis of these manually drawn contours, the maximal extent of GTV motion in the superoinferior direction was measured as ~12.5 mm.

Figure 4 shows the GTV centroid trajectory relative to the 4D-CT mean position extracted from five of the respiratory phases. Note the phase shift between the internal tumor and abdominal surface motion. The 0% phase corresponded to inhalation as recorded on the patient's abdominal surface with the RPM system and the most inferior position of the tumor was observed in the 20% phase volume. The large displacement of the GTV centroid on the light breathing scan (dashed lines) indicates that this scan was unrepresentative for the actual tumor position/volume. Breathing shuffles the anatomic slices, resulting in severe distortions of the tumor shape, as previously shown in Fig. 3. Table 1 summarizes the volumetric variations of the manually contoured GTV. The mean GTV throughout the 4D-CT image data was 21.7 cm^3 (standard deviation, 2.6 cm^2; 11.8%). The composite GTV derived from the union of 10 breathing phases was 39.9 cm^3. The GTV on the light breathing scan (24.4 cm^3) was comparable to the 4D-CT GTVs, although significant motion artifacts distorted the tumor shape.

Table 1. Volume of liver and lung tumor obtained by manual contouring on helical CT scan and 4D-CT volumes

Scan/phase	Liver tumor volume (cm^3)	Lung tumor volume (cm^3)
Helical CT, light breathing	296.68	24.35
4D-CT 0%	246.38	19.10
4D-CT 20%	275.46	21.20
4D-CT 40%	248.53	19.65
4D-CT 60%	257.22	23.94
4D-CT 80%	253.68	24.91

Abbreviation: 4D-CT = four-dimensional computed tomography.

Target volumes for a second lung tumor patient are shown in Fig. 5. GTVs were manually contoured on the light breathing scan, as well as on the 0% and 50% phases of the 4D-CT volumes. CTVs were generated by uniform 1-cm expansions to include possible microscopic tumor cell spread. The light-breathing PTV (uniform margins, 1 cm from CTV) was not representative of the actual volume needing treatment. This PTV barely covered the 4D-CT CTVs. Geometric miss of the CTV could be expected in this example because no further margin remained to account for possible setup errors and/or interfractional mean tumor position variations. Furthermore, the light-breathing PTV was significantly asymmetric and encompassed more normal lung tissue than needed.

Rapid segmentation of lung tumors: MIV

Figure 6 shows the MIV for the lung tumor in Fig. 3. MIVs rely on pronounced density differences between tumor and neighboring structures and therefore seem appropriate for lung tumors. Note the blurring of other structures in the lung parenchyma of the MIV CT image compared with the time-resolved images of lung in Fig. 3. The GTV of the MIV was 34.51 cm^3 compared with the 39.85-cm^3 composite GTV obtained by fusion of 10 manually contoured data sets. This difference was in part attributed to

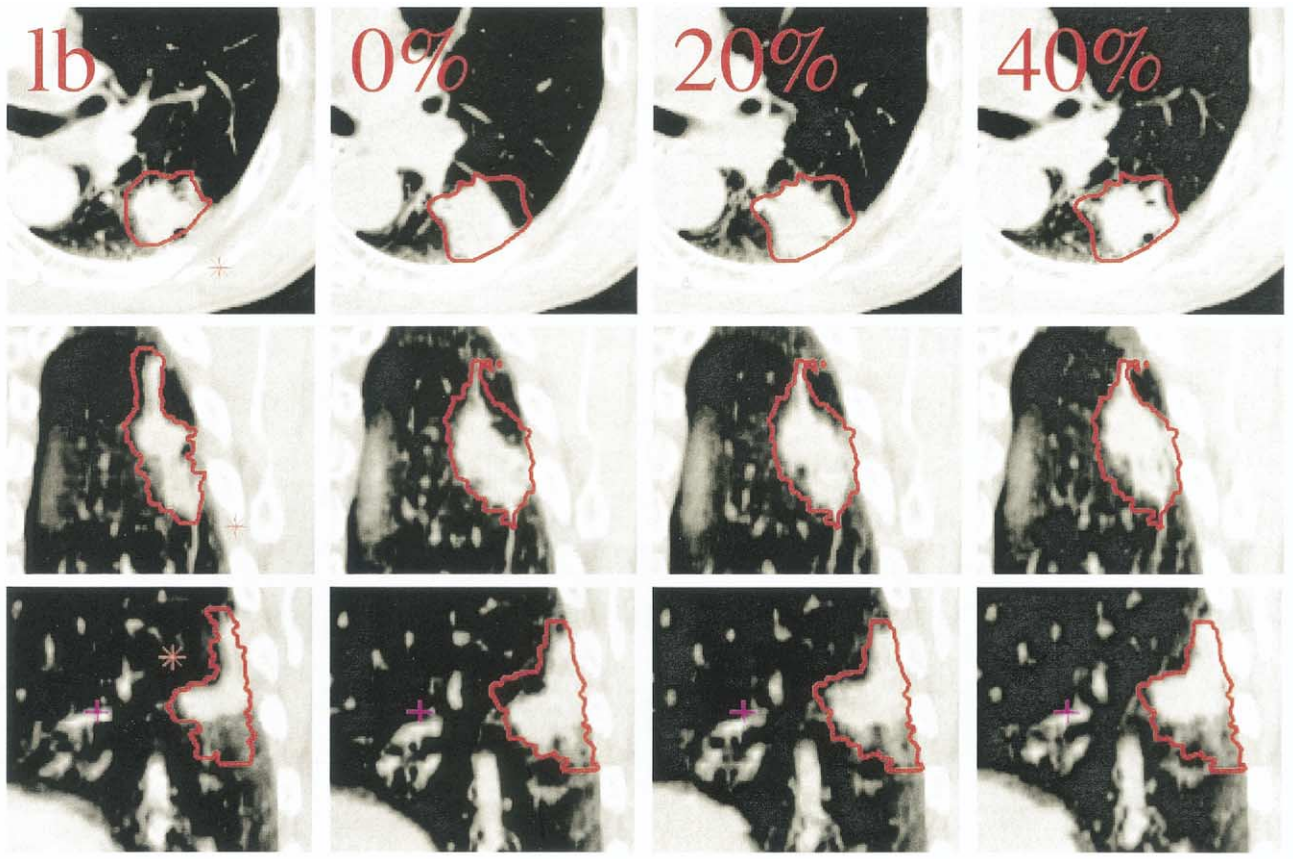

Fig. 3. Lung tumor motion axial (top), coronal (middle), and sagittal (bottom). Columns show standard helical computed tomography (CT) scan acquired during light breathing (lb) and phases of four-dimensionsal (4D)-CT data (0%, 20%, 40%). 4D-CT volumes display tumor motion, as well as significant reduction in breathing artifacts. Contours on 4D-CT data show union of 4D gross target volumes. (4D-CT: 140 peak-kilo-voltage, 40 milli-Ampere, 12 images/slice, 0.977 $\times$ 0.977 $\times$ 2.5 mm^3).

variations in manual contouring, because they were merged when combining 10 contour sets. This case also illustrates the potential for problems with an MIV approach if tumors are adjacent to the chest wall. It is possible that for some 4D-CT data sets, the chest wall moves anteriorly. The higher density of the chest wall tissue compared with the tumor can mask a small portion of the tumor in the MIV. Such obscured regions of the tumor will also lead to a reduction of the MIV in comparison with the composite GTV. However, for these tumor locations, typical expansions of the GTV to CTV would likely include the entire GTV and, in most cases, no margin expansion beyond the pleura would be necessary.

Figure 7 displays a single axial plane and multiple manually drawn GTV contours of the lung tumor. The light green contour defines the GTV obtained from manually contouring the tumor on the light respiration helical CT scan. Gray contours define the GTV as contoured on 5 of the 10 different respiratory phase CT scans. These instances document that the GTV moves well beyond the perceived boundary of the GTV from the light breathing scan. The red MIV contour encompasses inhale, exhale and nearly all intermediate 4D-CT breathing phases. Small differences at the anterior edges of the MIV require additional analysis, but were believed to be due to variations in manual contouring. MIVs were generated for three lung tumors in different patients, and visual validation of the results showed adequate inclusion of the tumor at all 4D-CT breathing phases.

Deformable image registration

Four-dimensional CT volumes at different phases of the patient's breathing cycle can be registered to a reference scan by deformable image registration, as described earlier. Although a detailed general validation of the nonrigid registration we have used has not been completed, individual case-specific results were validated on a slice-by-slice comparison between the target and deformed volume. Slices in the axial, sagittal, and coronal view were compared either as color overlays or by difference images. Such axial and coronal difference images are shown in Fig. 8.

Displayed are the input and difference images of nonrigid registration of the left lung and associated tumor adjacent to the posterior chest wall. The initial processing included the union of segmentations of both lung and tumor. The 40% respiratory phase lung volume was registered with the 0%

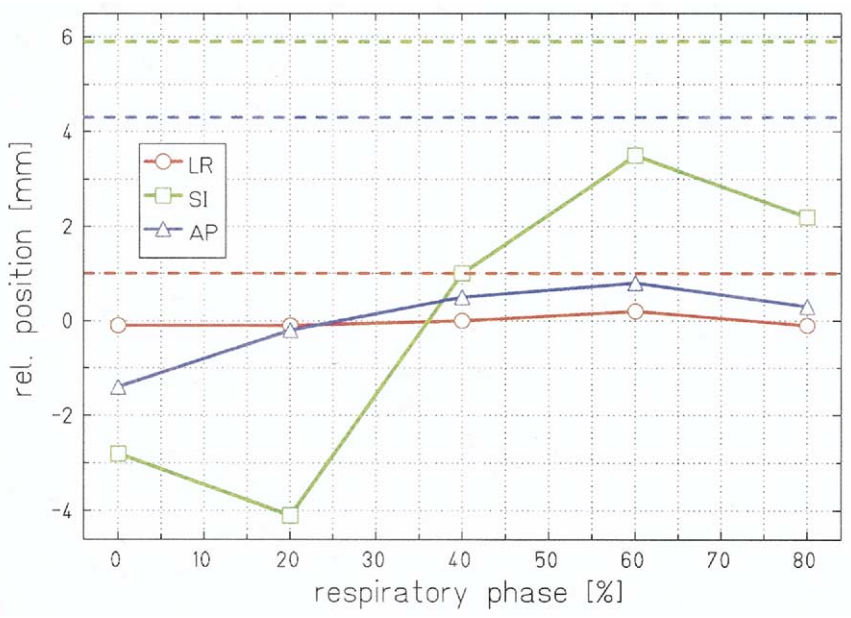

Fig. 4. Center of gross target volume (GTV) motion for lung tumor obtained from delineation on five respiratory phases; directions of motion: right positive, superior positive, and anterior positive. GTV centroid position from standard helical computed tomography (CT) scan acquired under light breathing indicated by dashed lines. Positions plotted relative to mean position from four-dimensional CT.

respiratory phase lung volume in full three dimensions. The top row shows the 0% phase original image (left) and the target 40% respiratory phase image (right). Subtraction images of differences before and after registration are shown in the bottom panel. The right half of Fig. 8 displays comparable data for the coronal section. Inspection of these difference images before and after registration showed the good performance of the algorithm, and differences were substantially reduced. Note the good agreement of the tumor after registration.

Registration performance can be limited by small residual imaging artifacts in the 4D-CT data sets (14), as well as by spatial resolution. Postregistration differences were visible, for example, in the circled region on the axial slices. The resolution of the CT volumes in the superoinferior direction was defined by the slice thickness (2.5 mm). The registration algorithm transformed the circled structure to the correct location within the resolution limit. Coronal difference images showed a comparable result; large differences existed at different respiratory phases before deformable registration but were significantly reduced after. The coronal post-registration difference image highlighted the depen-

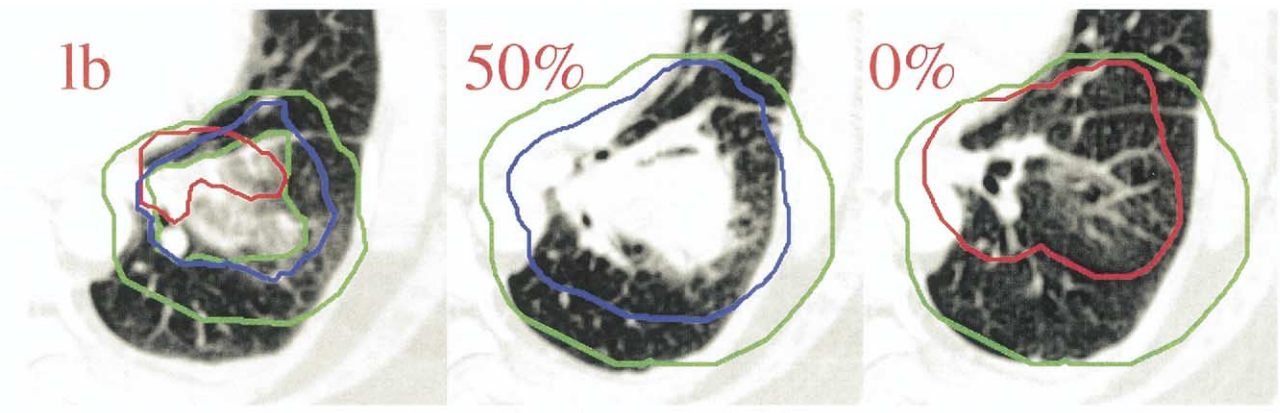

Fig. 5. Different target volumes for lung tumor: light breathing (green), four-dimensional computed tomography (4D-CT) 50% (blue), 4D-CT 0% (red). Left to right: (*1*) helical CT scan acquired under light breathing, light breathing gross target volume (GTV) and clinical target volume (CTV), 4D-CT GTVs at 0% and 50%; (*2*) 4D-CT 50% phase, light breathing planning target volume (PTV), 4D-CT GTV at 50%; (*3*) 4D-CT 0% phase, light breathing PTV, 4D-CT GTV at 0%. (4D-CT: 140 peak-kilo-voltage, 120 milli-Ampere, 16 images/slice, $0.977 \times 0.977 \times 2.5$ mm^3).

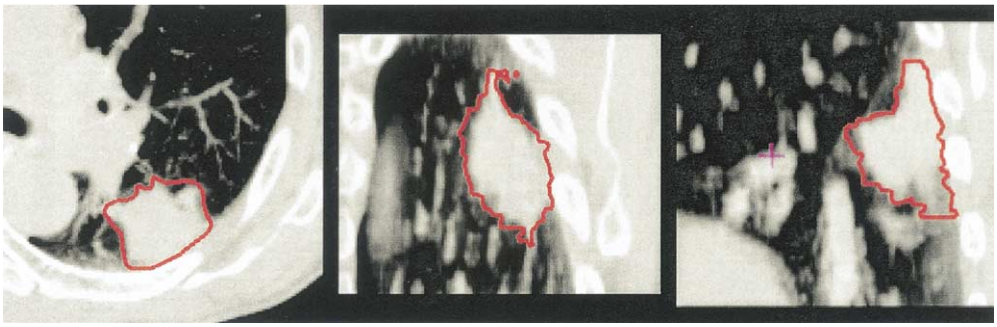

Fig. 6. Maximum intensity volume of lung tumor for fast contouring of composite gross target volume.

dency on z axis resolution; most of the residual differences were within one slice thickness. The black and white rims surrounding the lung primarily arose from differences in the initial segmentations on different respiratory volumes. These segmentations differed slightly at the lung periphery because of partial volume effects and possible residual imaging artifacts. Owing to volumetric interpolation during registration and transformation, the density edges were blurred in the transformed images. The image registration transformation vectors to register the 40% volume to 0% phase are shown in Fig. 9. A comparison of Figs. 7 and 9 shows the 3D nature of motion and deformation. Contours on transaxial cross-sections of the tumor varied more than indicated by the transformation vectors in the transaxial plane. Transaxial target cross-sections primarily varied because of superoinferior tumor motion, not deformation.

Dose calculations

A 3D conformal photon treatment plan for the lung tumor in Fig. 3 (five beams, 6 MV) was generated on the basis of the standard helical CT scan. After standard treatment planning approaches, 1-cm margins were applied to the GTV to generate a CTV; 1-cm margins were in turn applied to the CTV to generate a PTV. A prescribed dose of 72 Gy (to the 100% isodose line) was specified for this case study. The treatment plan was optimized to provide 100% isodose

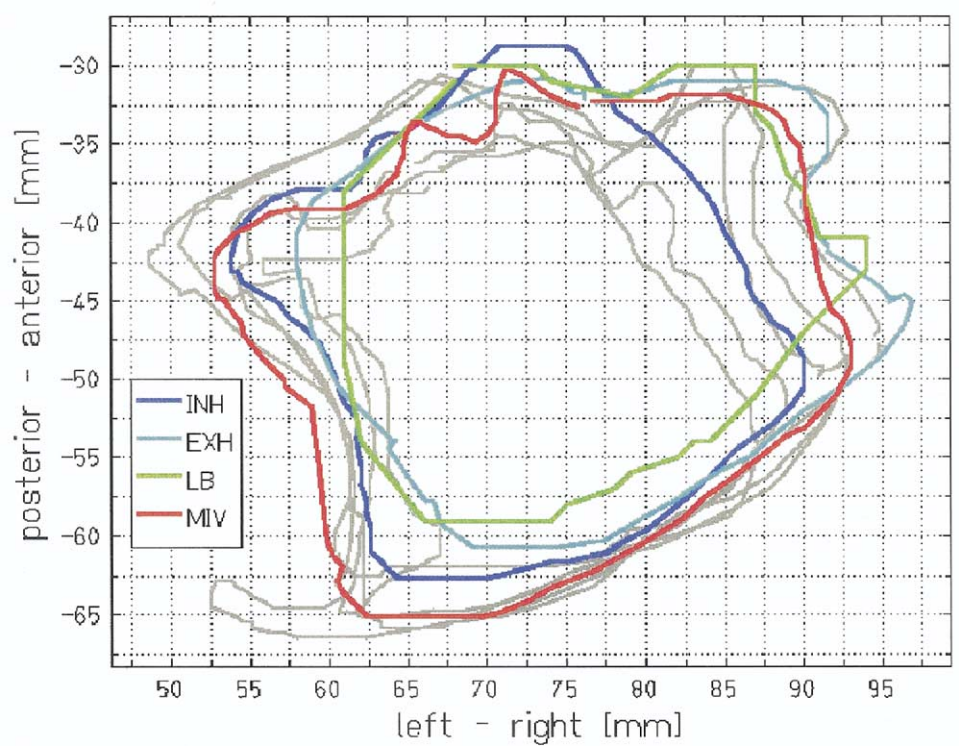

Fig. 7. Contour comparison for central axial cut through lung tumor. Contours shown for helical scan acquired during light breathing (LB), inhale breath hold (INH), and exhale breath hold (EXH). Based on four-dimensional computed tomography (4D-CT) data, maximum intensity volume was calculated and contoured. In addition, contours for five phases of 4D-CT data shown (light gray).

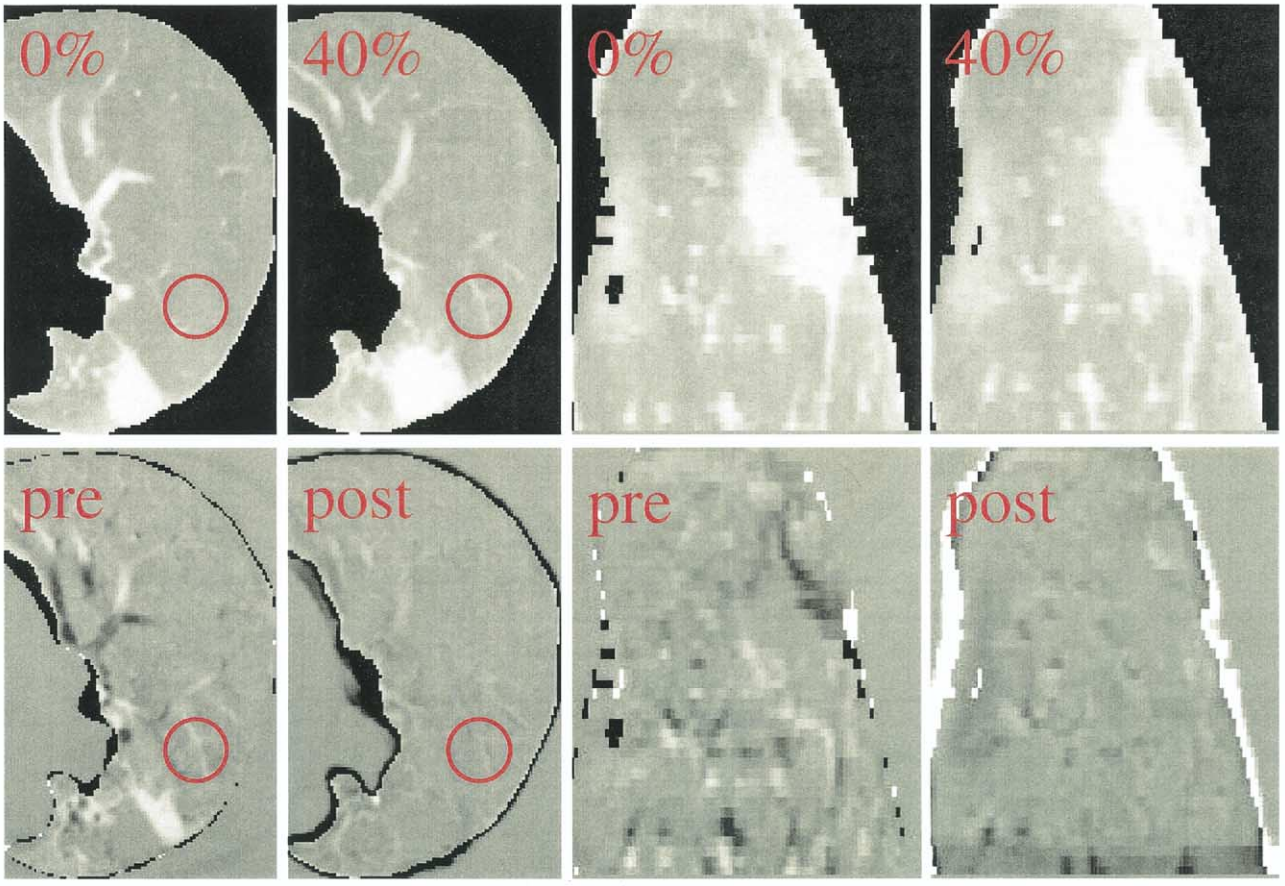

Fig. 8. Results of nonrigid lung registration showing axial and coronal slices of 0% and 40% four-dimensional computed tomography (4D-CT) volumes, as well as difference images before and after registration (using VTK CISG Registration Toolkit [23]). Registration results depended, among other factors, on the accuracy of 4D-CT imaging. Difference images show good performance of registration.

coverage of the CTV and a minimum of 95% isodose coverage of the PTV. Figure 10 displays the dose distributions calculated for the different respiratory phases. The top row of images of Fig. 10 show that the anatomic changes resulted in small dose perturbations. Variations in the spatial dose distribution between different respiratory phases within the CTV were within ±2% (using the FOCUS convolution algorithm for dose calculations). Engelsman *et al.*

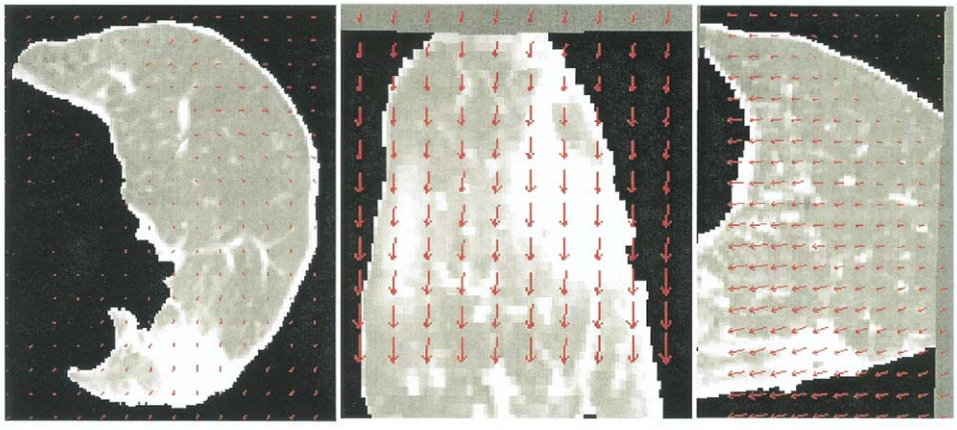

Fig. 9. Deformation fields for left lung and tumor from 40% (close to exhale) to 0% (close to inhale) respiratory phase four-dimensional computed tomography data (left to right: axial, coronal, sagittal).

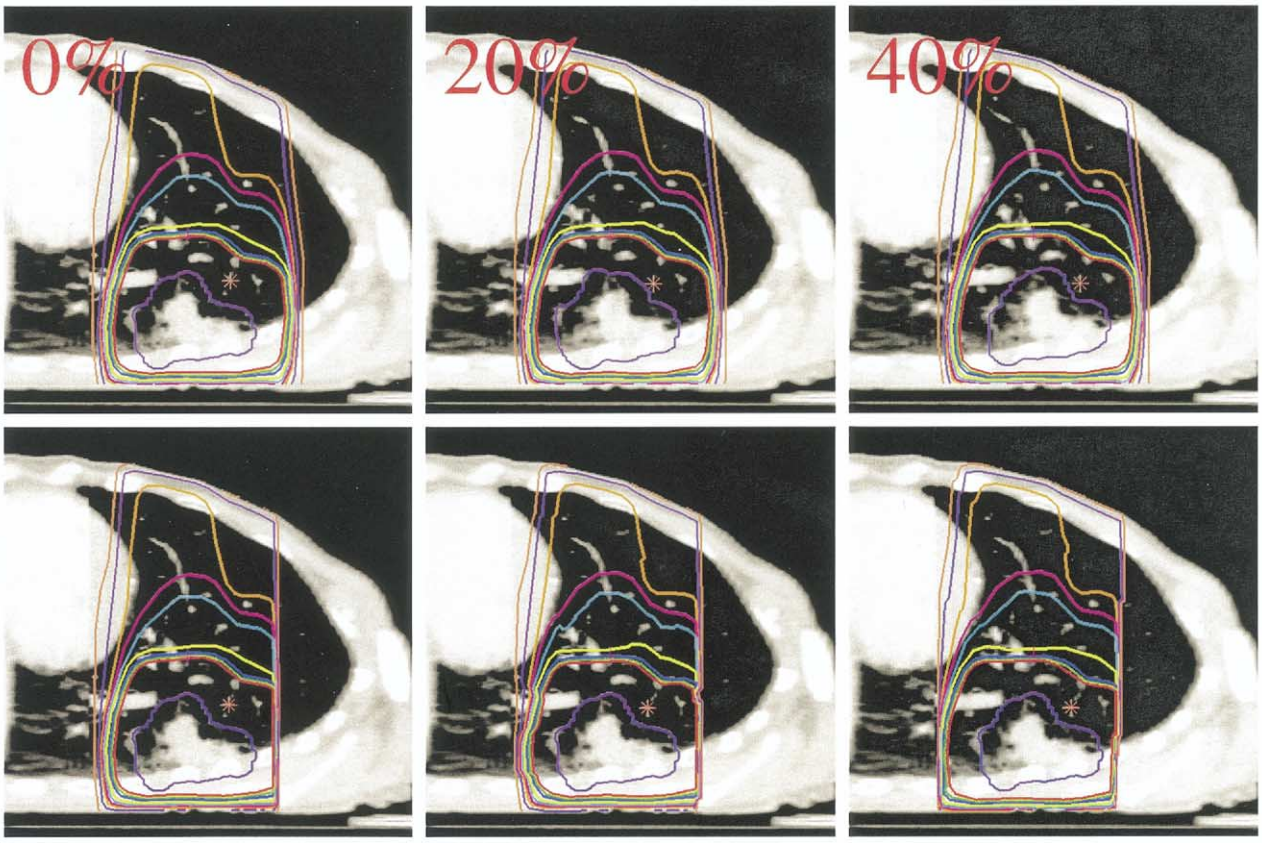

Fig. 10. Impact of organ motion (respiratory phases 0%, 20%, 40%) on dose distribution for 3D-conformal radiotherapy (RT) (top row; 6 MV, five beams, gantry angles 0°, 52°, 104°, 156°, 208°) and mapping dose distributions on 0% breathing phase computed tomography (CT) (bottom row). Deformations obtained by nonrigid CT–CT registration of corresponding respiratory phases (prescription dose 72 Gy). Relative isodose lines: red 99%, green 95%, blue 90%, yellow 80%, cyan 70%, magenta 60%, orange 50%, purple 30%, and brown 10%.

(25) reported similar results for phantom studies. Therefore, a quasistatic dose cloud could be assumed throughout the respiratory cycle. The underlying anatomy changes and the quasistatic dose was deposited at different anatomic locations from respiratory phase to phase within the irradiated area. Anatomic changes could be best observed by comparing distances between the CTVs and high isodose lines. To date, 4D dose distributions have been analyzed for 6 lung cancer patients. Similar results have been obtained and will be reported in more detail elsewhere.

The bottom images in Fig. 10 show the dose distributions at different respiratory phases when deformably mapped onto the CT data set closest to inhalation. The deformation parameters obtained from nonrigid CT–CT lung registration were used to map the dose distributions to the CT volume at inspiration respiratory phase, maintaining the dose-to-voxel correspondence. Deformation parameters were obtained between different 4D-CT volumes only; therefore, the dose distributions had to be clipped at the padding interfaces described above. This resulted in an unnatural sharp dose cutoff superior to the CTV. Mapping the dose distributions to the 0% breathing phase visualized the changes in dose deposition from phase to phase. In this frame of reference, the anatomy was static, but the dose distributions were dynamic. The distances between the CTV and isodose lines remained constant compared with the previous images.

Dose volume histograms calculated at the different respiratory phases are shown in Fig. 11 (dashed lines). This plot shows that the CTV was irradiated to 100% of the prescribed dose throughout the respiratory cycle. However, compared with the light breathing DVH, DVHs at the different respiratory phases indicated a reduced dose to the CTV. Recalling that the treatment plan was optimized for light breathing, in this case, departure from the static geometry to moving anatomy resulted in different dose to the target. Equivalent uniform doses (EUDs) for the CTV were calculated per respiratory phase and did not show significant differences. The EUDs were between 75.7 (0%) and 76.6 (40%) Gy. The EUD for the initial light breathing CTV was 76.2 Gy.

The dashed lines in Fig. 11 represent DVHs calculated on different 4D-CT data sets. The DVHs shown in solid lines were derived from transforming and registering the dose distributions to the 4D-CT data set closest to inhale. After deformable registrations have been applied, DVHs for different respiratory phases can be calculated on inhale anatomy using the inhale CTV. The agreement between the solid and dashed lines shows the good performance of the

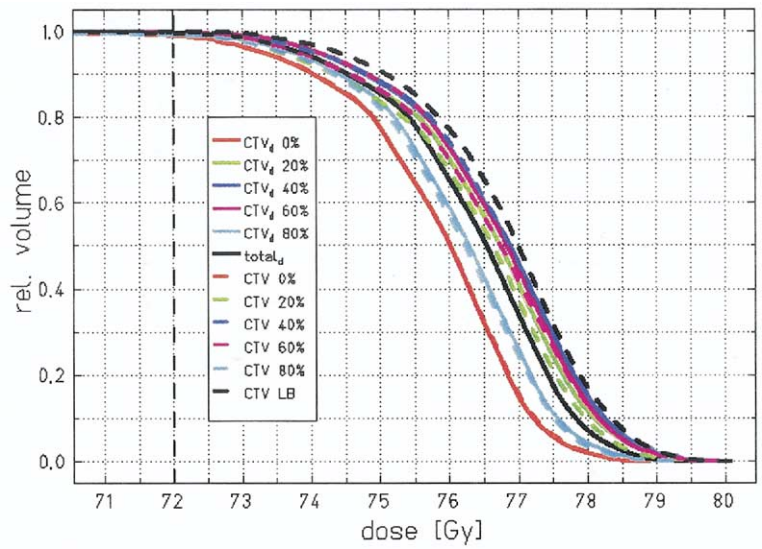

Fig. 11. Clinical target volume (CTV) dose volume histograms (DVHs) for different respiratory phases. Dashed lines show DVHs obtained on different four-dimensional computed tomography (4D-CT) data sets. DVHs in solid lines obtained by nonrigid deformations of dose distributions to data set closest to inhale, parameters obtained by CT–CT registration for different respiratory phases. Solid black line shows effective total DVH for patient, including respiration.

registration process. The DVHs shown as solid lines were calculated on the inhale data set using the inhale CTV. The agreement with the DVHs calculated on the original respiratory phases, without transforming dose distributions, highlights that the dose-to-voxel relation was maintained by the nonrigid transformations. The maximal difference between the corresponding DVHs at 50% volume was 0.1 Gy. The effective dose under respiratory motion was calculated by adding the transformed dose distributions on the inhale volume. The EUD for the CTV was 76.7 Gy.

The dose calculations above were performed assuming no setup errors or interfractional mean target position variations. According to ICRU 62 (9) recommendations, PTVs should account for intra- and interfractional target motion, as well as setup errors. Intrafractional target motion was included in the 4D-CT data. Consequently, the PTVs were generated per respiratory phase by uniform CTV expansions to incorporate the remaining sources of error. DVHs calculated assuming CTV to PTV expansions ranging from 1 to 15 mm in steps of 1 mm were generated. For expansions up to 3 mm, good coverage was maintained for all respiratory phases. Figure 12 shows the PTV DVHs for a 7-mm ex-

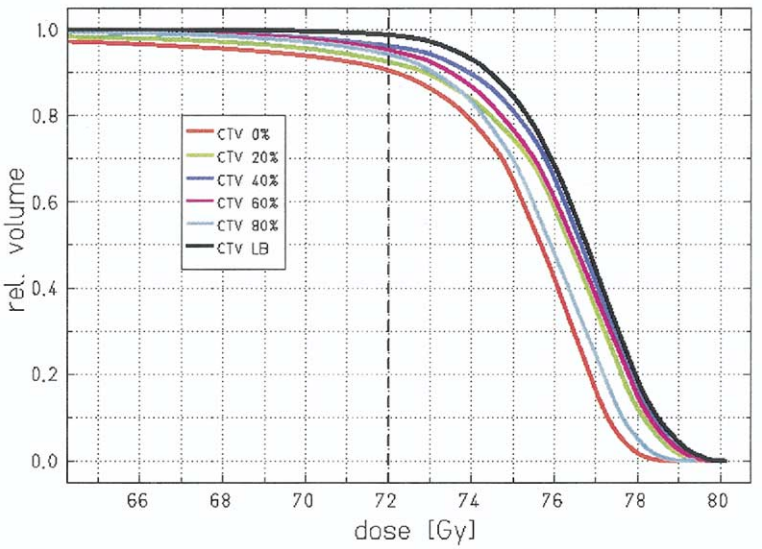

Fig. 12. Planning target volume (PTV) dose volume histograms (DVHs) for five respiratory phases of four-dimensional computed tomography data and standard helical scan, uniform clinical target volume to PTV expansions of 7 mm.

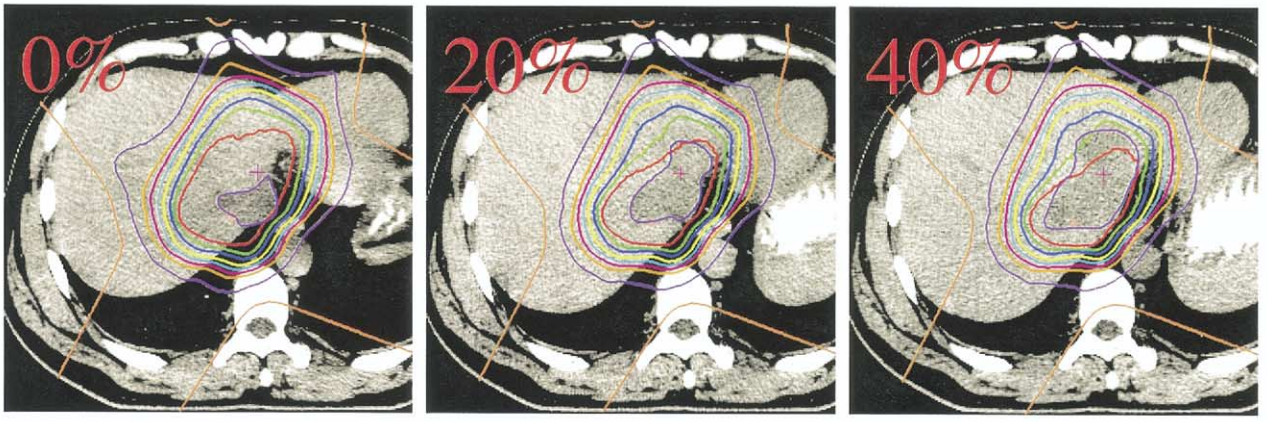

Fig. 13. Impact of organ motion (breathing phases 0%, 20%, 40%) on dose distributions for protons (four fields, gantry angles 20°, 115°, 210°, 315°); prescription dose 60 Gy. Relative isodose lines: red 99%, green 95%, blue 90%, yellow 80%, cyan 70%, magenta 60%, orange 50%, purple 30%, and brown 10%.

pansion. Inspection of this plot showed that for the light breathing nominal treatment plan, full target coverage was maintained. However, the prescribed dosimetric coverage for all 4D-CT respiratory phases was decreased to levels between ~96% and 90% volume. When imaging artifacts affecting target shape and location have not been fully taken into account, it is possible that a dosimetric consequence (underdose) can occur. Coverage of the initial nominal CTV could be expected because a 1-cm expansion to generate a PTV was applied.

A four-field proton treatment plan was optimized on a standard axial CT scan for the liver patient shown above. Dose distributions applying this nominal plan were then recalculated over anatomy at the different respiratory phases. Figure 13 shows the dose distributions on a transaxial cut for different breathing phases. In contrast to dose distributions from photons, proton dose distributions were significantly affected by anatomic changes. The discrete ranges of the Bragg peaks strongly depend on the density within the beam path. When the stomach and spleen move into the displayed axial slice during respiration, high-value isodose lines are shifted back toward the entrance surface owing to the increased density in the path of the left posterior oblique beam. Perturbations of the three other proton beams were relatively small, because the radiographic pathlength remained relatively stable for those portals. In these dose calculations, the oral contrast in the stomach was segmented and its density reset to unity to model more realistically the range perturbation. This temporal variation in anatomy emphasizes the importance of precise knowledge about organ motion, especially for charged particle therapy. Significant changes in range can be introduced by organ motion.

DISCUSSION

As shown in Fig. 14, the major tasks in 4D-RT are fundamentally the same as those in 3D-RT currently in practice. The workflow involves the key tasks of image acquisition, target delineation, and treatment planning and delivery. However, the process can be significantly more involved in its most explicit implementation. Image acquisition is marginally more complex. Data acquisition involves monitoring the respiratory cycle during CT scanning, but the total time typically required to take a 4D-CT scan is about 2–3 min. CT scan reconstruction of the 1500+ images is longer, but is not a rate-limiting step. Retrospective sorting of images into spatiotemporal coherent volumes can be performed in about 10 min. The sorting process is fully automated. The respiratory trace should be examined to estimate the quality of the 4D-CT data set on the basis of the breathing regularity (14).

More significant differences potentially arise in the image segmentation step. In 4D treatment planning, we are dealing with approximately 10 times more image data. Although in the research mode, manual segmentation is still the reference standard until machine vision algorithms to segment tissues automatically have been developed. It remains to be seen whether delineation of the gross target volume in the 4D image data can be achieved. That automated target delineation algorithms in 3D image data are not available suggests that this is a difficult problem. However, there may be some simpler approaches to dealing with the increased image data. We have illustrated several approaches to generate composite targets when indicated: in the case of lung tumors, the concept of the MIV may be useful; alternatively, segmentation of the extrema GTV at inhale and exhale, interpolating or merging to creating a composite GTV, and dynamically overlaying intermediate respiratory image data may simplify the process. Because of the possible phase shifts, extreme GTV positions have to be assessed from internal anatomy instead of the respiratory phase. If radiopaque markers can be implanted near the tumor, asymmetric margin expansions can be applied according to marker trajectories. Accounting for small hysteresis effects should be incorporated. Another method to propagate contour sets between respiratory states is based on nonrigid registration techniques. If CT data sets have been registered,

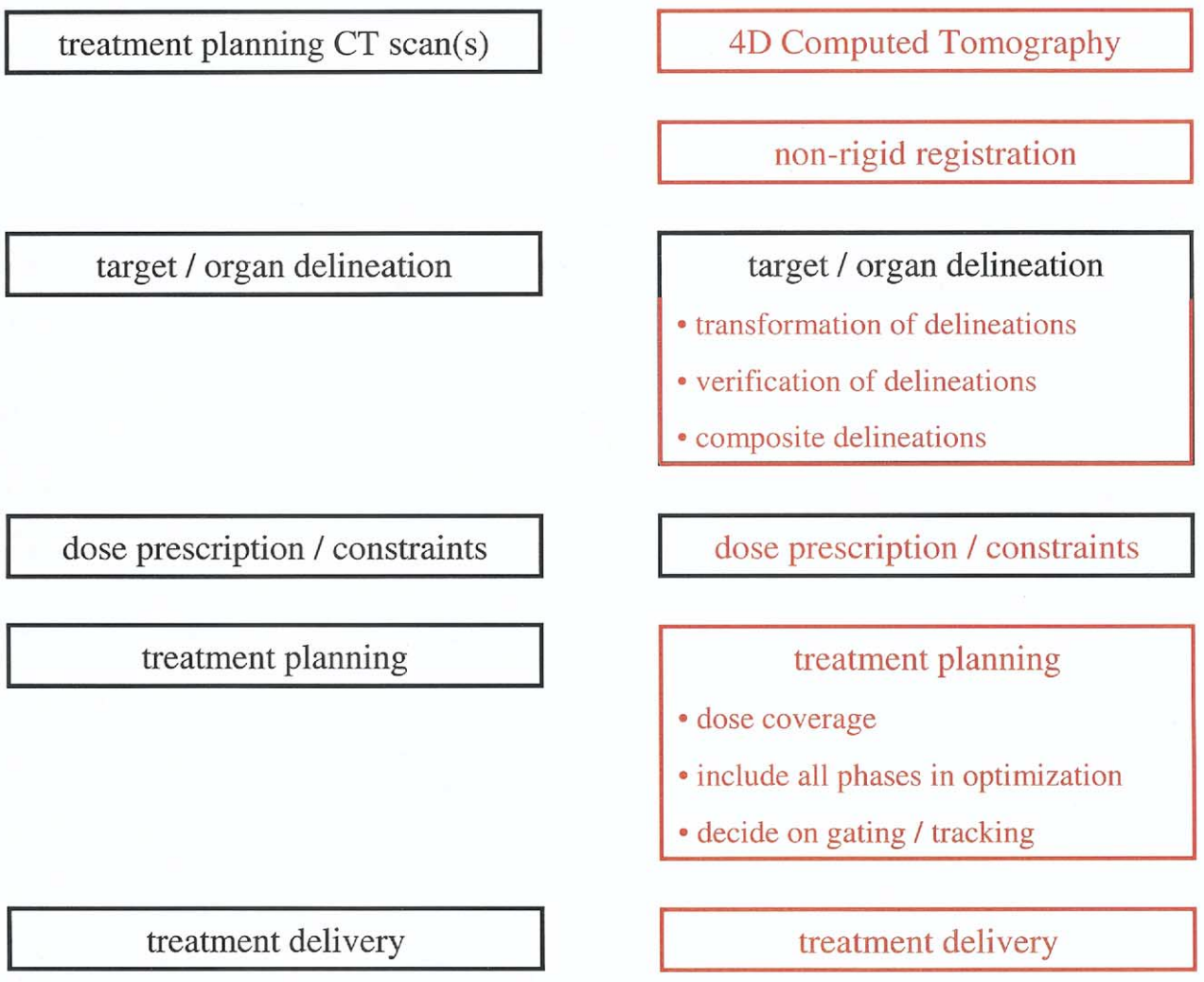

Fig. 14. Explicit inclusion of respiratory motion in treatment planning: Comparison between current workflow (left) and four-dimensional workflow (right).

contours can be morphed accordingly. If the registration of complete organs is not needed, only tumor segmentations can be registered between CT data sets. The significantly smaller tumor volume compared with complete organs will result in a significant decrease of computation time. Comparisons of manually contoured and transformed tumor segmentations are currently under investigation to assess the accuracy of nonrigid registration techniques.

Nonrigid registration of 4D-CT data sets can be used to study the dose not only during tumor motion, but also the dose to moving normal lung or other normal organs. In the lung study presented, a registration was computed for the entire scanned volume treated as a single entity. The registration results in this situation were poor (data not shown). Specifically, portions of the moving tumor, adjacent to the chest wall, could not correctly be registered to different respiratory phases because of its proximity to the static chest wall and ribs. Lung and surrounding chest wall move independently of each other at the pleura interface. Free-form deformation models, implemented by B-splines, cannot adequately accommodate abrupt changes in the deformation field. Improved deformable registration was achieved by separately considering the moving organs (lung, tumor) from the minimally moving/static organs (chest wall, ribs, spine).

Dose calculation in the full implementation of 4D treatment planning is likewise complex. Deformable image registration is an important component of this step, because it enables the mapping of dose from multiple anatomic maps at different instants of time to a common geometry. The accuracy of the registration method we used needs to be analyzed and validated. Brock *et al.* (26) reported registration accuracy of about 1–1.4 mm using thin-plate splines for mutual information-based warping between livers at the exhale and inhale positions. Nonrigid registration facilitates the accurate calculation of DVHs in the presence of voxel displacement during respiration. Although nonrigid registration was considered successful for the segmented lung, we could not calculate the lung DVHs under breathing motion owing to the limited scan length. An order of mag-

nitude increase in dose calculation time is needed, given the corresponding increase in image data. If nonrigid registration is not available, dose coverage analysis of the target for all respiratory phases seems appropriate. DVHs per respiratory phase can be computed to ensure coverage. If targets were not outlined on all data sets, visual inspection can be used. With dynamic beam delivery systems, interplay effects should be studied in more detail. In our current implementation, the interplay between dynamic beam delivery and organ motion was not explicitly included to simplify the initial IMRT dose calculations. IMRT doses were calculated as if all fields were delivered simultaneously by a 3D compensator.

If dose distributions are calculated including respiratory motion, dose prescriptions and constraints have to be carefully evaluated. Current standard values are based on experience that did not explicitly include motion. We presented changes in DVHs for a lung tumor. For additional studies, 4D imaging of the whole lung is planned to assess the dosimetric changes for normal lung tissues. For photon treatments, the motion of lung tissue within a quasistatic dose distribution leads to a blurring of the deposited dose; accurate DVHs will be assessable.

Finally, advances in treatment delivery techniques are needed. Development of tracking, image-guided therapy, and verification of target motion on a daily basis would be required to ensure that the motion as planned is indeed reproducible within acceptable limits of dose uncertainty.

Given the significant increase in complexity when performing 4D scanning and treatment planning, what are the potential benefits? The additional knowledge can be used to estimate more rationally the target volume shape and trajectory. This will lead naturally to an evidence-based choice of the appropriate treatment technique. Ideally, the appropriate treatment technique will be chosen on the basis of comparisons of the dose delivered in the presence of motion. Constraints such as multicollimator leaf widths and so forth should be explicitly included in the decision process. Because some residual motion is likely to occur, regardless of technique (e.g., gating window, uncertainties in breath hold), 4D techniques provide insight into the effects of such motions on the dose. For gating techniques, the most favorable respiratory phases can be obtained by dosimetric comparisons and phase shifts between the external surface and internal target motion can directly be included.

Earlier work has shown that the uncertainty of GTV extent in the craniocaudal axis can be twice the amplitude of the periodic motion (3) when the scan is performed in helical mode during light respiration. A specific example was the visualization of a 6-cm sphere that was shortened to 4 cm longitudinally when undergoing 1-cm amplitude periodic motion. Such imaging errors cannot be corrected except by large target expansions, which lead to an unfavorable increase in unnecessary irradiated normal tissue. With 4D imaging, this uncertainty can be reduced to one slice thickness at each end of travel, or 2.5 mm with commonly used scan parameters. Furthermore, in contrast to breath-hold CT scans, the organ motion is imaged.

The 4D planning approach provides direct tumor visualization on a patient-specific basis. Estimates of tumor motion from four dimensions are far superior to what can be extracted from fluoroscopic analysis, especially for those sites in which radiopaque clips are not common (such as the lung). Because the patient breathes naturally, one can argue that the extrema at inhale and exhale are more representative than those obtained by breath hold at these points, although more data are needed to verify this. Combined with fluoroscopic clip data, 4D modeled motion may provide insight into the dose delivered under realistic breathing for periods of minutes, in which the observed amplitude and frequency variations are incorporated into the calculation. We must point out that the 4D dose calculations strongly depend on the patient's respiratory cycle. If the amplitude changes significantly, dosimetric changes will occur.

As a research tool, 4D treatment planning on multiple cases can provide insight into how such respiratory motions affect the dose to each voxel. This is an interesting question, given dynamic beam delivery techniques such as IMRT and beam tracking approaches. Adaptive RT, and the associated dose calculations, are fundamentally 4D planning in a broader sense. The explicit examination of radiographic pathlength to targets undergoing charged particle RT is of particular interest to the growing number of proton RT facilities.

The possibility of 4D treatment planning naturally leads to considering how to optimize dose distributions in the presence of motion. Optimization here can include calculations that might reveal at what respiratory phase one could irradiate the tumor most confidently and spare the most amount of normal tissue. What are the tradeoffs between gating and tracking? How can we optimize the fluence pattern in IMRT to be robust in the presence of motion? Especially for dynamic beam delivery, additional precise studies are needed to characterize the impact of interplay effects between organ motion and beam delivery.

Four-dimensional treatment planning in principle provides more accurate dose calculations when organs move during treatment. The technology for imaging and dose calculation is becoming available. Currently, 4D planning and delivery are in their initial phase of research and development. 4D treatment delivery will require innovative technological advances. This article has outlined some of the key issues that need to be dealt with for 4D imaging and treatment planning. We have used these new capabilities for treatment planning of some patients at MGH.

CONCLUSION

We have demonstrated the feasibility of explicitly incorporating patient-specific 4D-CT imaging data in external beam treatment planning. To achieve this, special attention was given to defining the target volumes in the time domain and to apply methods to perform deformable

registration during respiration. New technical challenges in performing 4D dose calculations include coping with 10–20 times more imaging data and the associated increase in image segmentation. The output of 4D planning are dynamic dose distributions, reflecting dose perturbations as a function of time. These distributions can be summed over time and space through temporal deformable image registration. The end result is, in principle, a more accurate assessment of the dose delivered to each voxel of the region of interest when organs move during respiration. The importance of this knowledge lies in an improved understanding of the interplay between organ motion and beam delivery methods such as IMRT or charged particle therapy. This knowledge is essential in devising approaches to optimally mitigate undesirable dose variations.

REFERENCES

1. Balter JM, Ten Haken RK, Lawrence TS, *et al.* Uncertainties in CT-based radiation therapy planning associated with patient breathing. *Int J Radiat Oncol Biol Phys* 1996;36:167–174.
2. Shimizu S, Shirato H, Kagei K, *et al.* Impact of respiratory movement on the computed tomographic images of small lung tumors in three-dimensional (3D) radiotherapy. *Int J Radiat Oncol Biol Phys* 2000;46:1127–1133.
3. Chen GT, Kung JH, Beaudette KP. Artifacts in computed tomography scanning of moving objects. *Semin Radiat Oncol* 2004;14:19–26.
4. Caldwell CB, Mah K, Skinner M, *et al.* Can PET provide the 3D extent of tumor motion for individualized internal target volumes? A phantom study of the limitations of CT and the promise of PET. *Int J Radiat Oncol Biol Phys* 2003;55:1381–1393.
5. Balter JM, Lam KL, McGinn CJ, *et al.* Improvement of CT-based treatment planning model of abdominal targets using static exhale imaging. *Int J Radiat Oncol Biol Phys* 1998; 41:939–943.
6. Ritchie CJ, Hsieh J, Gard MF, *et al.* Predictive respiratory gating: A new method to reduce motion artifacts on CT scans. *Radiology* 1994;190:847–852.
7. Balter JM, Dawson LA, Kazanjian S, *et al.* Determination of ventilatory liver movement via radiographic evaluation of diaphragm position. *Int J Radiat Oncol Biol Phys* 2001;51:267–270.
8. International Commission on Radiation Units and Measurements. ICRU report 50: Prescribing, recording and reporting photon beam therapy. Bethesda: ICRU; 1993.
9. International Commission on Radiation Units and Measurements. ICRU report 62: Prescribing, recording and reporting photon beam therapy (supplement to ICRU report 50). Bethesda: ICRU; 1999.
10. Langen KM, Jones DT. Organ motion and its management. *Int J Radiat Oncol Biol Phys* 2001;50:265–278.
11. Stevens CW, Munden RF, Forster KM, *et al.* Respiratory driven lung tumor motion is independent of tumor size, tumor location, and pulmonary function. *Int J Radiat Oncol Biol Phys* 2001;51:62–68.
12. Van Sörnsen de Koste JR, Lagerwaard FJ, Nijssen-Visser MRJ, *et al.* Tumor location cannot predict the mobility of lung tumors: A 3D analysis of data generated from multiple CT scans. *Int J Radiat Oncol Biol Phys* 2003;56:348–354.
13. Rosu M, Dawson LA, Balter JM, *et al.* Alterations in normal liver doses due to organ motion. *Int J Radiat Oncol Biol Phys* 2003;57:1472–1479.
14. Rietzel E, Pan T, Chen GTY. 4D computed tomography: Image formation and clinical protocol. *Med Physics* 2005; in press.
15. Vedam SS, Keall PJ, Kini VR, *et al.* Acquiring a four-dimensional computed tomography data set using an external respiratory signal. *Phys Med Biol* 2003;48:45–62.
16. Ford EC, Mageras GS, Yorke E, *et al.* Respiration-correlated spiral CT: A method of measuring respiratory-induced anatomic motion for radiation treatment planning. *Med Phys* 2003;30:88–97.
17. Low DA, Nystrom M, Kalinin E, *et al.* A method for the reconstruction of four-dimensional synchronized CT scans acquired during free breathing. *Med Phys* 2003;30:1254–1263.
18. Pan T, Lee TY, Rietzel E, *et al.* 4D-CT imaging of a volume influenced by respiratory motion on multi-slice CT. *Med Phys* 2004;31:333–340.
19. Ramsey CR, Scaperoth D, Arwood D, *et al.* Clinical experience with a commercial respiratory gating system. *Int J Radiat Oncol Biol Phys* 2000;48:164–165.
20. Wagman R, Yorke E, Giraud P, *et al.* Reproducibility of organ position with respiratory gating for liver tumors: Use in dose-escalation. *Int J Radiat Oncol Biol Phys* 2003;55:659–668.
21. Vedam SS, Kini VR, Keall PJ, *et al.* Quantifying the predictability of diaphragm motion during respiration with a noninvasive external marker. *Med Phys* 2003;30:505–513.
22. Allen AM, Siracuse KM, Hayman JA, *et al.* Evaluation of the influence of breathing on the movement and modeling of lung tumors. *Int J Radiat Oncol Biol Phys* 2004;58:1251–1257.
23. Hartkens T, Rueckert D, Schnabel JA, *et al.* VTK CISG Registration Toolkit: An open source software package for affine and non-rigid registration of single- and multimodal 3D images. In: Meiler M, Saupe D, Kruggel F, *et al.* editors. Bildverarbeitung für die Medizin 2002, Algorithmen–Systeme–Anwendungen. Workshop Proceedings, Leipzig March 2002, Series: Informatik aktuell. Leipzig: Springer-Verlag; 2002.
24. Rueckert D, Sonoda LI, Hayes C, *et al.*Non-rigid registration using free-form deformations: Application to breast MR images. *IEEE Trans Med Imaging* 1999;18:712–721.
25. Engelsman M, Damen EM, De Jaeger K, *et al.* The effect of breathing and set-up errors on the cumulative dose to a lung tumor. *Radiother Oncol* 2001;60:95–105.
26. Brock KK, McShan DL, Ten Haken RK, *et al.* Automated generation of a four-dimensional model of the liver using warping and mutual information. *Med Phys* 2003;30:1128–1133.